Centre Européen de Recherche et de Formation Avancée en Calcul Scientifique

Beyond Boolean logic. A family of logistic equations as a model for numerical evolution of the fixed points 0 and 1 for multiplication

M. Monserrat Rincon-Camacho, Françoise Chatelin and Philippe Ricoux

Technical Report TR/PA/14/68

Publications of the Parallel Algorithms Team

http://www.cerfacs.fr/algor/publications/

BEYOND BOOLEAN LOGIC. A FAMILY OF LOGISTIC EQUATIONS AS A MODEL FOR NUMERICAL EVOLUTION OF THE FIXED POINTS 0 AND 1 FOR MULTIPLICATION

M. MONSERRAT RINCON-CAMACHO [(1),(2)], FRANÇOISE CHATELIN [(1),(2)], AND PHILIPPE RICOUX [(3)]

Abstract. We study the fixed-point equation, given for fixed $l > 0$ by:

$$y = 1 - m|y|^l, \quad y, m \in \mathbb{R}, \tag{1.1}$$

where $|y|$ represents the absolute distance of y to 0. Eq. (1.1) induces a duality between 0 and 1, elements of $\mathbb{Z}_2$. We indicate that this duality can be interpreted, in the context of logic, as a paradox. We analyse the theoretical behaviour for $l \in \mathbb{N}^*$ and the experimental results for $0 < l < 1$. This work is to be compared with the study of the fixed-point equation given by $x = h(1 - |2x - 1|^l)$, $h, x \in \mathbb{R}$ presented in CERFACS TR/PA/14/55.

Keywords: Fixed points 0, 1 for real multiplication, absolute distance to 0, logistic family, wavetracks, forward chaos, 2-cycle, liar paradox, first incompleteness theorem of Gödel.

1. Introduction

1.1. **A family of logistic equations.** In this work we are interested in the family of logistic equations for $l > 0$ given by

$$y = 1 - m|y|^l = 1 - me^{l \ln |y|} = G_l(m, y), \quad m \in \mathbb{R}, \tag{1.1}$$

which appears in [Briggs, 1991]. We aim to make a study similar to the one presented in [Rincon-Camacho et al., 2014a] for the logistic equations

$$x = h\Lambda_l(x), \quad \Lambda_l(x) = 1 - |2x - 1|^l. \tag{1.2}$$

When $l = 2$, equation (1.2) becomes the well known classical logistic equation

$$x = 4hx(1 - x), \quad h \in \mathbb{R} \tag{1.3}$$

heavily studied between 1970 and 1990, [Feigenbaum, 1979, May et al., 1974, Nagashima and Baba, 1999].

The case $l = 2$ in (1.1) provides the fixed point equation

$$y = 1 - my^2 = G_2(m, y). \tag{1.4}$$

In Figure 1 (a), we see in red the fixed points corresponding to the intersection of the curves $z = y$ (in black) and $z = 1 - my^2$ for different values of m. There are no real intersections of these curves when the parabola $z = 1 - my^2$ is above the bisector $z = y$ which occurs for the case $m \leq -\frac{1}{4}$. Indeed in Section 2.2 we see that equation (1.4) is satisfied when $m \geq -\frac{1}{4}$

(1) CEREMATH, Université Toulouse 1, 21, Allée de Brienne, 31000 Toulouse, France. (rincon@cerfacs.fr).
(2) CERFACS, 42, avenue Gaspard Coriolis, 31057 Toulouse, France. (chatelin@cerfacs.fr).
(3) TOTAL SA Direction Scientifique, 24, cours Michelet LA DEFENSE 10, 92069 Paris La Defense CEDEX, France. (philippe.ricoux@total.com).

by $y_{(1)}(m) = \frac{-1+\sqrt{1+4m}}{2m}$ or $y_{(2)}(m) = \frac{-1-\sqrt{1+4m}}{2m}$. The equation (1.4) should be related to the better-known real Mandelbrot equation

$$x = m - x^2 \quad \Leftrightarrow \quad x^2 + x - m = 0 \tag{1.5}$$

whose real solution for $m \geq -\frac{1}{4}$ is the parabola $x(m) = \frac{1}{2}(1 \pm \sqrt{1+4m})$. Hence $y(m) = \frac{x(m)}{m}$.

The value 1 is either a maximum of the quadratic function $f_m(y) = 1 - my^2$ when $m \geq 0$ or a minimum when $m < 0$, in both cases this extremum occurs at the critical value $y = 0$.

The way the parabolas $G_2(m, y) = 1 - my^2$ and $h\Lambda_2(x) = 4hx(1-x)$ vary depending on the parameters m and h is remarkably different. In Figure 1 (a), we observe that m in $G_2(m, y)$ affects the radius of curvature but keeps 1 as the extreme value $G_2(m, 0)$ whereas h modifies the extreme value $h\Lambda_2(\frac{1}{2})$. See [Rincon-Camacho et al., 2014a, Section 1.1] for a more detailed description of $h\Lambda_2$. In Figure 1 (b), the behaviour of the fixed point iteration

$$y_0 = 0, \;\; y_{n+1} = 1 - m|y_n|^l, \; n \geq 0, \tag{1.6}$$

for $m \geq -\frac{1}{4}$ and $l = 2$ is illustrated. For m equal to -0.15, 0.15, 0.25, and 0.65 the iterates y_n reach a steady state after some iterations n, contrary to the value 1.45 where y_n continuously oscillates. These convergence results are assembled in the orbit diagram depicted in Figure 1 (c) when $200 \leq n \leq 400$ and the initial condition is given by $x_0 = \frac{1}{2}$.

As we mentioned before, in this report we analyse the fixed point equation (1.1) together with the Picard iteration (1.6) in order to better understand the information processing displayed by this general family of logistics as we did for the logistic equations (1.2) in [Rincon-Camacho et al., 2014a].

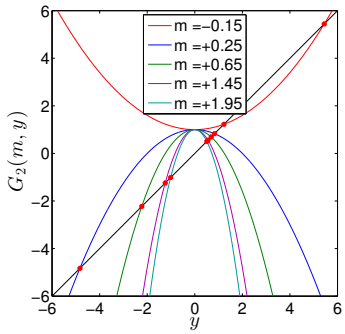

(a) fixed points $y = G_2(m, y)$

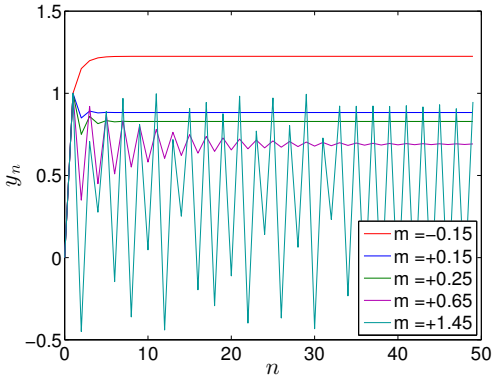

(b) iteration map $n \mapsto y_n$

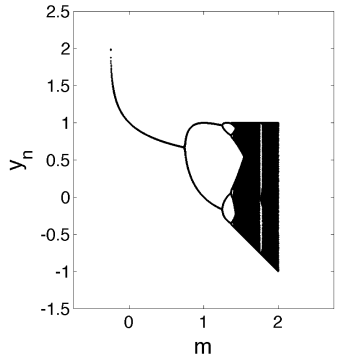

(c) orbit diagram ($200 \leq n \leq 400$)

FIGURE 1. Dynamics of the logistic equation $y = 1 - my^2$, $-\frac{1}{4} \leq m \leq 2$

In Figure 2, we plot the function $G_l(1, y) = 1 - |y|^l$ for different values of l. The shape of the function $G_l(1, y)$ for $y \in [-1, 1]$ is similar to that of $\Lambda_l(x) = 1 - |2x - 1|^l$ for $x \in [0, 1]$, see [Rincon-Camacho et al., 2014a, Section 1.1]. In both cases the maximum value is 1, in $G_l(1, y)$ it is achieved for $y = 0$ and in $\Lambda_l(x)$ it is achieved when $x = \frac{1}{2}$.

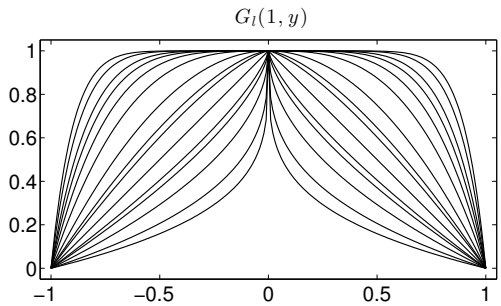

FIGURE 2. $G_l(1, y)$ for $l = \frac{1}{4}, \frac{1}{3}, \frac{1}{2}, \frac{2}{3}, \frac{3}{4}, 1, \frac{4}{3}, \frac{3}{2}, 2, 3, 4, 5, 6, 8, 10$, $y \in [0, 1]$

However, a main difference between (1.2) and (1.1) is that in orbit diagrams of (1.2), $l \geq \frac{1}{2}$, exhibit backward *and* forward chaos (i.e. chaos for h in two disjoint intervals) and the

orbit diagrams of (1.1) exhibit only forward chaos. The dynamics of the law of composition depends on the *domain* of *definition* of the real solutions to the fixed point equations. In (1.1) $m \mapsto y(m) \in \mathbb{R}$ consists of two branches, one defined for $m \geq m_0$, $m_0 < 0$, and the other for $m > 0$. By comparison the solutions of (1.2) are defined on *unbounded* domains. The difference is computationally *significant*. Thus it is puzzling to realise that this major difference has not attracted the attention of the many scientists working in the field of one dimensional discrete dynamical systems. Theory tells us that the condition $S(G_l) < 0$ should hold at least *locally* for pitchfork bifurcations to occur, defining Feigenbaum's route to chaos.

Lemma 1.1. *The sign of $S(G_l)$ is that of $1 - l^2$ for $y \neq 0$, $m \neq 0$.*

Proof. By direct computation. Set $f(y) = 1 - m|y|^l$. For $y > 0$, $f = 1 - my^l$, $f' = -mly^{l-1}$, $f'' = -ml(l-1)y^{l-2}$, $f''' = -ml(l-1)(l-2)y^{l-3}$. Therefore the sign of $S(f) = \frac{f'''}{f'} - \frac{3}{2}(\frac{f''}{f'})^2 = \frac{1}{f'^2}[f'f''' - \frac{3}{2}(f'')^2]$ is that of $m^2l^2(l-1)y^{2(l-2)}\frac{-l-1}{2}$, or equivalently, that of $-(l-1)(l+1) = 1-l^2$. The same result holds for $y < 0$, $f(y) = 1 + my^l$. This confirms that $S = 0$ for $l = 1$ and $S < 0$ for $l > 1$.

□

1.2. **Beyond Boolean logic.** We have shown in [Rincon-Camacho et al., 2014a, Section 1.3] that the fixed points of (1.2) are analogue of 0 and 1, the fixed points of **1** which define the Boolean logic, a quantitative model for Aristotle's logic [Boole, 1854]. The same report addressed the replacement of **1** by $h\Lambda_l = h(1 - |2x-1|^l)$ where $|2x-1| = \frac{|x-\frac{1}{2}|}{\frac{1}{2}}$ is the *relative* distance to $\frac{1}{2} = \frac{0+1}{2}$. In the present work, **1** is replaced by $G_l(m, y) = 1 - m|y|^l$ where $|y|$ is the *absolute* distance to 0. Section 1.3 below develops some logical consequences of the occurrence of an absolute distance in G_l.

1.3. **An absolute evolution of numbers.** Here we consider (1.1) as a model for the numerical evolution of the fixed points 0 and 1 for multiplication under the variation of the parameter m. Equation (1.1) expresses that the distance $|y|$ from y to 0 raised to the power l, is equal to the relative distance $\frac{1-y}{m}$, that is

$$|y|^l = \frac{1-y}{m}, \quad m \neq 0.$$

The quotient $\frac{y-1}{m} = \frac{y(m)-y(0)}{m-0}$ is a divided difference whose value is $\tan\psi(m)$ where $\psi(m)$ is the angle displayed on Figure 3.

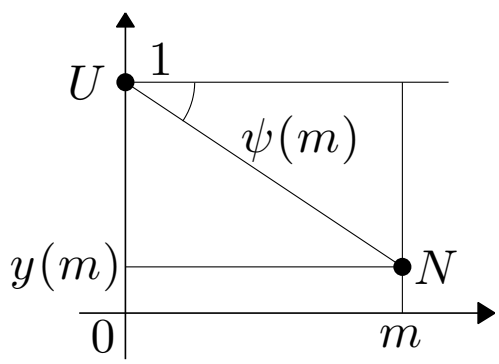

FIGURE 3. The angle $\psi(m)$

The point $N = (m, y(m))$ on the curve $m \mapsto y(m)$ is seen from the point $U = (0, 1)$ under the angle $\psi(m)$. We notice that $|y|$ is an absolute distance to 0 and that the information in (1.1) is provided by 0 and 1 only.

Eq. (1.1), rewritten as $-|y|^l = \tan \psi(m)$, tells us that the deviation of $y(m)$ from 1, that is of $\psi(m)$ from 0, is quantified by $-|y|^l$, the opposite of the *absolute* distance to 0 raised to the power $l > 0$. Since $1 \neq 0$, Eq. (1.1) introduces a *duality* between 0 and 1: 0 if 1 and 1 if 0. The two answers are equally valid but mutually incompatible. The situation cannot be expressed by the fixed point of (1.1) but, rather, by its 2-cycle which solves $y = G(m, G(m, y))$. The celebrated first incompleteness theorem of Gödel is based upon this 2-cycle through the Gödel sentence: "this statement is not provable within the formal axiomatic system under consideration". See [Gödel, 1931] and its english translation [Hirzel, 2000]. Gödel's theorem says in essence that Arithmetic is an incomplete theory, a statement which would not have surprised any Pythagorean of the $6^{\underline{\text{th}}}$ century BC. As this is recalled in [Chatelin, 2015, pp. 171-172] Gödel was well aware that his incompleteness theorems were the consequences of the *static* nature of the chosen formal axiomatic system. One way out of any logical dilemma is to *change* the point of view. A logical version of the 2-cycle which is non technical is given by the *liar paradox*: "this statement is false", which goes back to Ancient Greece and Epimenides the Cretan, famous for his claim that: "All Cretans are liars!" That the human mind is not immune to such paradoxes is illustrated by the two famous Gestalt pictures displayed by Figure 4.

(a) 1 vase or 2 profiles? (b) young or old lady?

FIGURE 4. Visual dilemmas

See [Rincon-Camacho et al., 2014a, Section 1.4] for a comparison with a relative evolution of numbers based on the fixed point (or 1-cycle) of (1.2).

1.4. **Organisation of the Report.** We make a theoretical study of the real roots of equation (1.1) for l integer, $1 \leq l \leq 4$ in Section 2 which refers to the Appendix in [Rincon-Camacho et al., 2014a]. The Picard iteration on (1.1) is contrasted with the explicit real solutions of (1.1) for $l \in \{1, 2, 3, 4\}$ in Section 3 and with computed real solutions for $0 < l < 1$ and $l \to \infty$ in Section 4. The wavetracks are introduced in Section 5. In Section 7 all numerical simulations for (1.1) are discussed and contrasted with those for (1.2) [Rincon-Camacho et al., 2014a]. The Feigenbaum constants α_l and δ_l, $l \in \mathbb{N}^*$, computed in [Briggs, 1991, Briggs, 1997] are presented in Section 6. Finally some preliminary conclusions are given in Section 8.

2. The exponent l as an integer in $\mathbb{N}^*$

The real solutions $y(m)$ of equation (1.1) are described in this section for $l \in \{1, 2, 3, 4\}$. The nature of the solutions, either real (distinct or double) or complex depends on the parameter m, this dependency on m is revealed thanks to the venerable methods of Cardano and Ferrari, see the Appendices A, B in [Rincon-Camacho et al., 2014a] which detail the survey given in [Bronstein and Semendiaev, 1990]. However on this report, we shall only consider the existence of real roots.

2.1. **Case $l = 1$.** For $l = 1$, equation (1.1) becomes $y = 1 - m|y|$. If $y \geq 0$, then $y = 1 - my$. Thus, the first part of the solution (displayed in blue in Figure 5 (a)) is given by

$$y_1 = \frac{1}{1+m}, \quad y_1(0) = 1$$

which satisfies $y_1 > 0$ when $m > -1$. If $y < 0$, then $y = 1 + my$ and we have that

$$y_2 = \frac{1}{1-m},$$

where $y_2 < 0$ if $m > 1$. This part of the solution is plotted in red in Figure 5 (a). In Figure 5 (b), the curve $m \mapsto \tan\psi(m)$ is displayed, showing that $-\frac{\pi}{2} < \psi(m) < 0$.

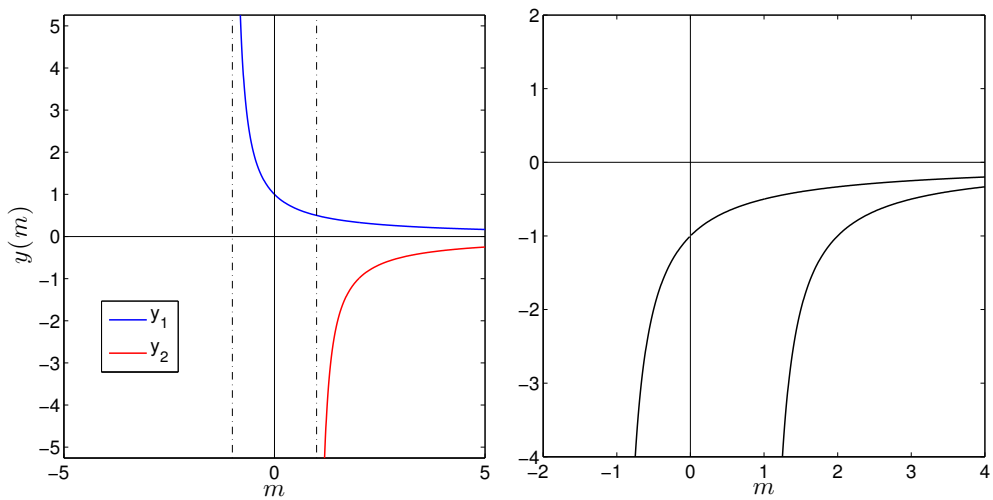

(a) $y(m)$ (b) $\tan\psi(m) = \frac{y(m)-1}{m}$

Figure 5. $l = 1$

2.2. **Case $l = 2$.** When $l = 2$, equation (1.1) becomes $y = 1 - my^2$ which was introduced in section 1.1. The solutions satisfy the following quadratic equation

$$my^2 + y - 1 = 0.$$

Here we see that the discriminant $\Delta = 1 + 4m$ is nonnegative if $m \geq -\frac{1}{4}$. The two solutions are then:

$$y_1 = \frac{-1 + \sqrt{1+4m}}{2m} > 0, \; y_1(0) = 1, \quad y_1(\tfrac{1}{4}) = 2,$$
$$y_2 = \frac{-1 - \sqrt{1+4m}}{2m} < 0,$$

plotted in blue and red respectively in Figure 6 (a). The quotient $\frac{y(m)-1}{m}$ is displayed in Figure 6 (b).

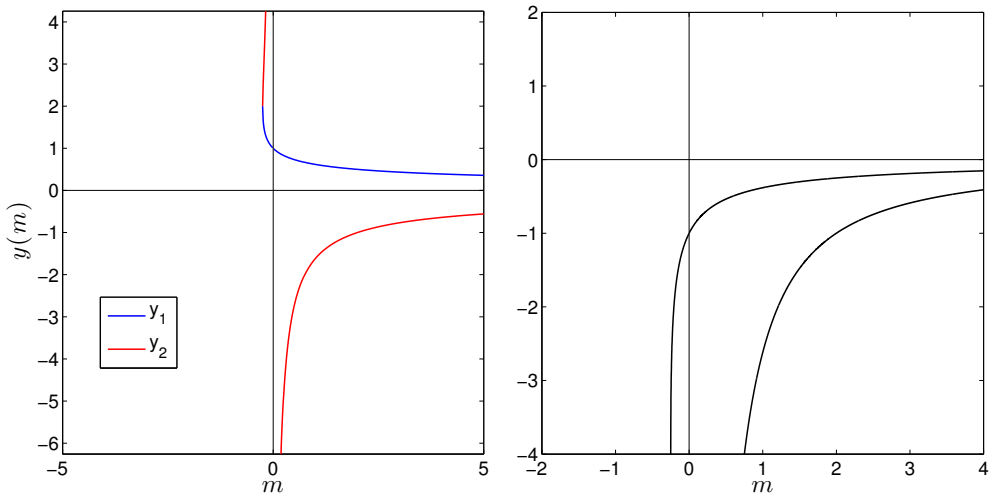

(a) $y(m)$, $m \geq -\frac{1}{4}$ (b) $\tan\psi(m) = \frac{y(m)-1}{m}$

FIGURE 6. $l = 2$, $m \geq -\frac{1}{4}$

2.3. **Case $l = 3$.** Due to the absolute value in $y = 1 - m|y|^3$ resulting from (1.1) when $l = 3$, we obtain two cubic equations for $y \geq 0$ and $y \leq 0$. We solve these equations by Cardano's method described in Appendix A.

2.3.1. $y \geq 0$. In this case the cubic equation to be solved has the following reduced form:

$$my^3 + y - 1 = 0 \;\Leftrightarrow\; y^3 + \frac{1}{m}y - \frac{1}{m} = 0,\; m \neq 0.$$

Hence $q(m) = -\frac{1}{2m}$, $p(m) = \frac{1}{3m}$ and the discriminant D which depends on m is given by:

$$D(m) = \frac{1}{m^2}\left(\frac{1}{3^3 m} + \frac{1}{2^2}\right) = \frac{1}{m^3}\left(\frac{1}{27} + \frac{1}{4}m\right).$$

Thus, the sign of $D(m)$ is derived in the following way with $m_0 = -\frac{4}{27} \approx -0.148$:

$$D(m) \geq 0 \quad \text{if} \;\; m \in]-\infty, m_0] \cup]0, \infty[,$$
$$D(m) < 0 \quad \text{if} \;\; m \in]m_0, 0[.$$

Clearly $q(m) > 0$ if $m < 0$, $q(m) < 0$ if $m < 0$ and $p(m) > 0$ if $m > 0$, $p(m) < 0$ if $m < 0$ and

$$\frac{q}{r^3} = \frac{|q|}{|p|^{3/2}} = \frac{1}{2|-m|} \cdot 3^{3/2}|m|^{3/2} = \frac{3^{3/2}\sqrt{|m|}}{2}$$

On the interval $]-\infty, m_0]$, $D(m) \geq 0$ and $p(m) < 0$, hence the real root is given by

$$y_1 = -2r\cosh\frac{\varphi}{3}$$

where φ is given by $\cosh\varphi = \frac{q}{r^3}$, but y_1 is not acceptable since $y_1 < 0$ as it is displayed by a dotted blue line in Figure 7. On the interval $]m_0, 0]$, $D(m) < 0$, hence there are three real solutions

$$y_1 = -2r\cos\frac{\varphi}{3}, \;\; y_2 = 2r\cos\frac{\pi - \varphi}{3}, \;\; y_3 = 2r\cos\frac{\pi + \varphi}{3},$$

respectively plotted as a dotted blue line, a green line and an orange line in Figure 7, only y_2 and y_3 satisfy the condition $y_2 \geq 0$ and $y_3 \geq 0$. Here φ is given by $\cos\varphi = \frac{q}{r^3}$. Finally on the interval $m \in]0, \infty[$, the discriminant is such that $D(m) > 0$ and $p(m) > 0$, thus $\sinh\varphi = \frac{q}{r^3}$ and there is only a real solution

$$y_1 = -2r \sinh\frac{\varphi}{3}$$

which is acceptable since $y_1 \geq 0$ as it may be seen in blue in Figure 7.

2.3.2. $y < 0$. In order to find the solution satisfying $y < 0$ we need to solve the following cubic equation in reduced form

$$my^3 - y + 1 = 0, \Leftrightarrow y^3 - \frac{1}{m}y + \frac{1}{m} = 0, \ m \neq 0.$$

We have that

$$q(m) = \frac{1}{2m}, \ p(m) = -\frac{1}{3m} \text{ and } D(m) = \frac{1}{m^2}\left(\frac{1}{2^2} - \frac{1}{3^3 m}\right) = \frac{1}{m^3}\left(\frac{1}{4}m - \frac{1}{27}\right).$$

$m_1 = \frac{2^2}{3^3} = -m_0 \approx 0.148$ the sign of $D(m)$ is as follows

$$\begin{aligned} D(m) \geq 0 \quad &\text{if } \ m \in]-\infty, 0[\cup[m_1, \infty[\\ D(m) < 0 \quad &\text{if } \ m \in]0, m_1[. \end{aligned}$$

We readily observe that $q(m) > 0$ if $m > 0$, $q(m) < 0$ if $m < 0$ and $p(m) > 0$ if $m < 0$, $p(m) < 0$ if $m > 0$ and we have that

$$\frac{q}{r^3} = \frac{|q|}{|p|^{3/2}} = \frac{1}{2|-m|} \cdot 3^{3/2}|m|^{3/2} = \frac{3^{3/2}\sqrt{|m|}}{2}.$$

When $m \in]-\infty, 0]$, $D(m) > 0$ and $p(m) > 0$, then the real root given by

$$y_1 = -2r \sinh\frac{\varphi}{3},$$

where $\sinh\varphi = \frac{q}{r^3}$. This solution, plotted as a dotted blue line in Figure 8, is not acceptable since $y_1 \geq 0$. In the interval $]0, m_0]$, we have that $D(m) < 0$, thus there are three real roots

$$y_1 = -2r\cos\frac{\varphi}{3}, \ \ y_2 = 2r\cos\frac{\pi - \varphi}{3} \ \text{ and } \ y_3 = 2r\cos\frac{\pi + \varphi}{3},$$

where only y_1 displayed in blue in Figure 8 is acceptable since it satisfies $y_1 < 0$ contrary to y_2 plotted as a dotted green line and y_3 plotted as a dotted orange line in Figure 8. Here φ is given by $\cos\varphi = \frac{q}{r^3}$. If $m \in]m_1, \infty[$, then $D(m) \geq 0$ and $p < 0$ and there is only one real root given by

$$y_1 = -2r\cosh\frac{\varphi}{3}$$

where $\cosh\varphi = \frac{q}{r^3}$. This solution is acceptable since $y_1 < 0$ as it may be observed in Figure 8. The final solution $y(m)$ of (1.1) when $l = 3$ is plotted in Figure 9, with $y(m_0) = \frac{3}{2}$, $y(0) = 1$.

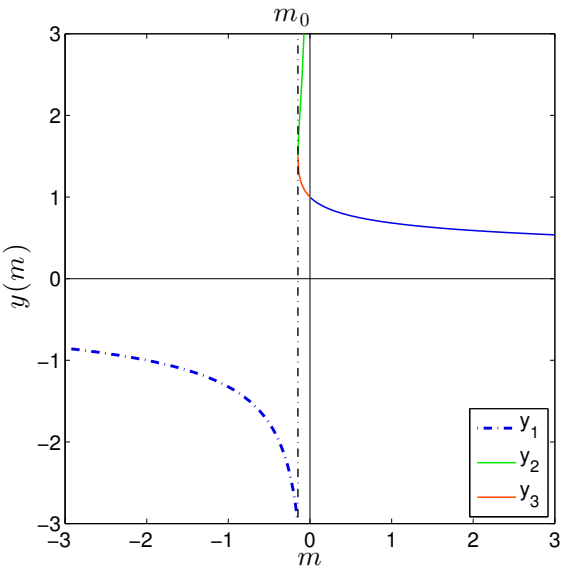

FIGURE 7. $y(m)$ for $l = 3$ and $y \geq 0$, $m_0 = -\frac{4}{27}$

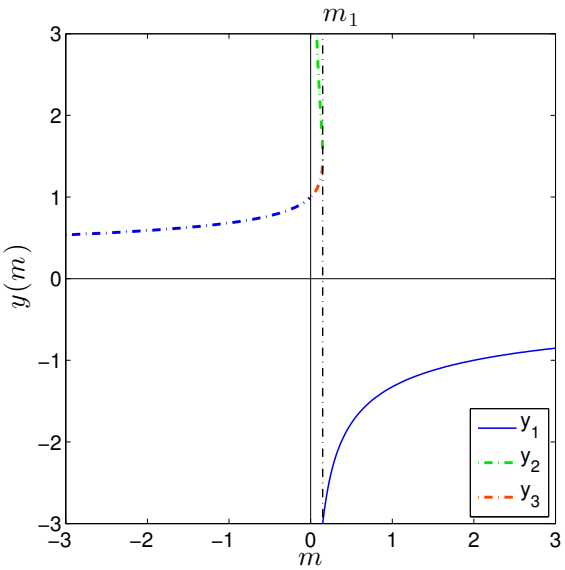

FIGURE 8. $y(m)$ for $l = 3$ and $y < 0$, $m_1 = \frac{4}{27}$

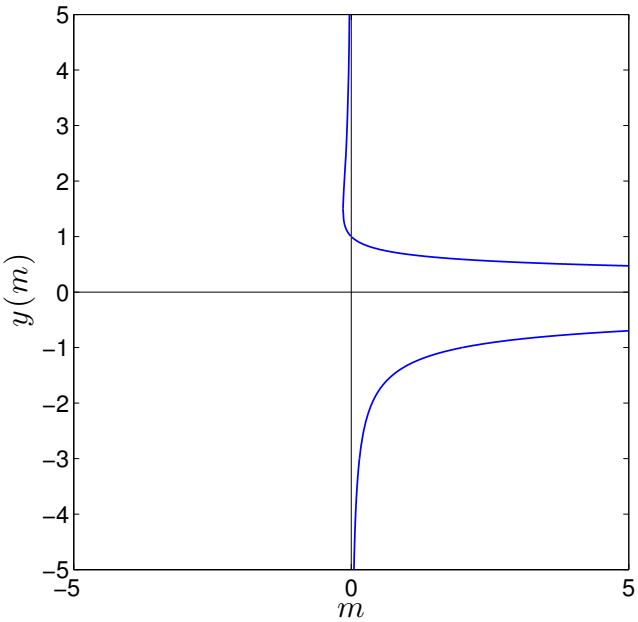

FIGURE 9. $y(m)$ for $l = 3$, $m \geq -\frac{4}{27}$

2.4. **Case $l = 4$.** . When $l = 4$ the absolute value in (1.1) is not necessary and we have $y = 1 - my^4$. The solution $y(m)$ is given by the roots of the following quartic equation

$$y^4 + \frac{1}{m}y - \frac{1}{m} = 0,\ m \neq 0. \tag{2.1}$$

We use Ferrari's method as described in Appendix B of [Rincon-Camacho et al., 2014a]. By substituting $b = 0$, $c = 0$, $d = \frac{1}{m}$ and $e = -\frac{1}{m}$ in (B.2), we have that

$$A = \pm\sqrt{8z} = \pm 2\sqrt{2z},$$

where z is a solution of the auxiliary cubic equation

$$8z^3 + \frac{8}{m}z - \frac{1}{m^2} = 0 \ \Leftrightarrow\ z^3 + \frac{1}{m}z - \frac{1}{8m^2} = 0. \tag{2.2}$$

In order to have $A \in \mathbb{R}^*$ it is necessary that $z > 0$, we refer to this condition as c_A. The cubic equation (2.2) is solved by Cardano's method. We obtain readily:

$$q(m) = -\frac{1}{2^4 m^2} < 0,\ \ p = \frac{1}{3m} \ \text{ and } \ D(m) = \frac{1}{m^3}\left(\frac{1}{3^3} + \frac{1}{2^8 m}\right) = \frac{1}{m^4}\left(\frac{1}{27}m + \frac{1}{256}\right).$$

Hence the sign of the discriminant $D(m)$ follows with $m_0 = -\frac{27}{256} \approx -0.1055$:

$$m \in]m_0, 0[\cup]0, \infty[,\quad D(m) > 0,$$
$$m \in]-\infty, m_0[,\quad D(m) < 0,$$

Moreover

$$r(m) = -\frac{1}{\sqrt{3|m|}},\ \ \frac{q}{r^3} = \frac{|q|}{|p|^{3/2}} = \frac{1}{2^4 m^2}\cdot 3^{3/2}|m|^{3/2} = \frac{3^{3/2}}{2^4|m|^{1/2}}.$$

If $m \in]-\infty, m_0[$ then $D(m) < 0$ and the cubic equation (2.2) has three real roots in this interval

$$z_1 = -2r\cos\frac{\varphi}{3},\ \ z_2 = 2r\cos\frac{\pi - \varphi}{3} \ \text{ and } \ z_3 = 2r\cos\frac{\pi + \varphi}{3},$$

where $\cos\varphi = \frac{q}{r^3}$. Only z_1 satisfies the condition c_A, i.e. $z_1 \geq 0$. In Figure 10, the solutions z_1, z_2 and z_3 are plotted in blue, as a dotted green line and a dotted orange line respectively. In the interval $m \in]m_0, 0[$, $D(m) > 0$ and $p(m) < 0$ thus there is only one real solution to equation (2.2) given by

$$z_1 = -2r\cosh\frac{\varphi}{3}$$

plotted in blue in Figure 10 which satisfies condition c_A. Here φ is such that $\cosh\varphi = \frac{q}{r^3}$. Finally if $m \in]0, \infty[$ then $D(m) > 0$ and $p(m) > 0$ and the unique real root is given by

$$z_1 = -2r\sinh\frac{\varphi}{3},$$

where $\sinh\varphi = \frac{q}{r^3}$. This solution is acceptable since it satisfies condition c_A and it is displayed in blue in Figure 10.

For the resulting $A = \pm 2\sqrt{2z}$, the quadratic equations are $w^2 \pm \sqrt{2z}w + z \pm \frac{1}{2m}\frac{1}{\sqrt{2z}} = 0$. The discriminants

$$\Delta_- = -2z - \frac{1}{m}\sqrt{\frac{2}{z}},\quad \Delta_+ = -2z + \frac{1}{m}\sqrt{\frac{2}{z}}$$

are plotted in blue and in green respectively in Figure 11. In order to obtain a real root for the quartic equation (2.1), the discriminants need to non negative. If $m \in]-\infty, m_0[$, none of the

discriminants is positive. If $m = m_0$, $\Delta_- = 0$ and $y_1 = y_2 = \sqrt{\frac{z}{2}} = \frac{4}{3}$. In the interval $m \in]m_0, 0[$ only Δ_- is positive and the corresponding real solutions are:

$$y_1 = \sqrt{\frac{z}{2}} + \frac{1}{2}\sqrt{\Delta_-} \quad \neq \quad y_2 = \sqrt{\frac{z}{2}} - \frac{1}{2}\sqrt{\Delta_-},$$

plotted in blue and green in Figure 12. If $m \in]0, \infty[$, only Δ_+ is positive and the solutions to (2.1) in this interval are

$$y_3 = -\sqrt{\frac{z}{2}} + \frac{1}{2}\sqrt{\Delta_+} \quad \neq \quad y_4 = -\sqrt{\frac{z}{2}} - \frac{1}{2}\sqrt{\Delta_+},$$

where y_3 is displayed in red and y_4 in brown in Figure 12.

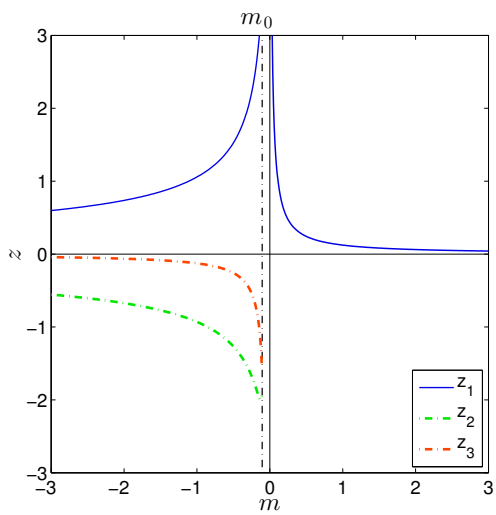

FIGURE 10. Solutions to equation (2.2)

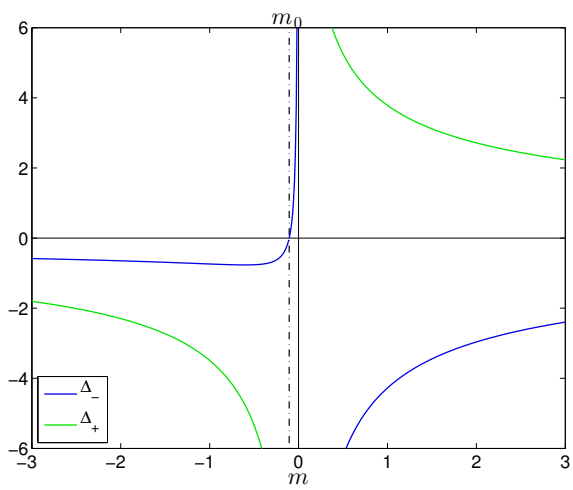

FIGURE 11. Δ_+ and Δ_-, $\Delta_-(m_0) = 0$

We observe that when $|m| \to \infty$, both coefficients of two quadratic polynomials tend to 0, since $\lim_{|m|\to\infty} \left(\frac{1}{|m|\sqrt{2z}}\right) = 0$. Ferrari's method provides the solution $y(\infty) = 0$ (with multiplicity 4) for (2.1) as expected.

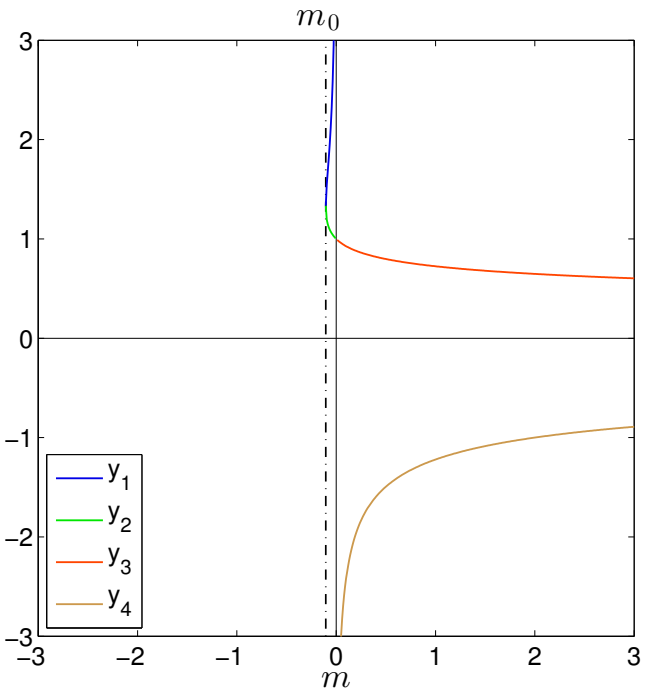

FIGURE 12. $y(m)$ for $l = 4$, $m \geq -\frac{27}{256}$

Finally, given the exact solutions $y(m)$ for $l = 3$ and $l = 4$, the quotient $\frac{1-y(m)}{m}$ is computed and displayed in Figure 13.

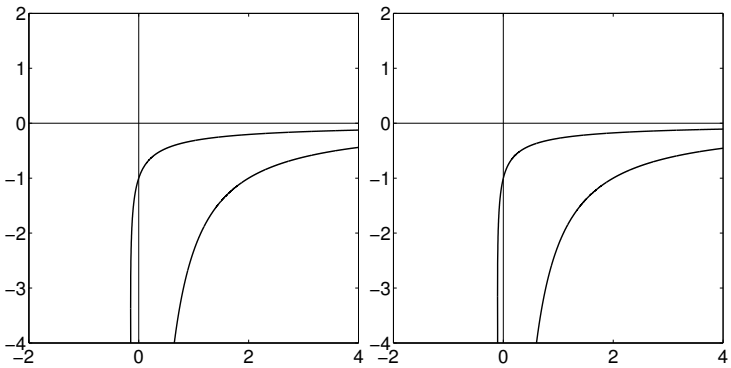

(a) $l = 3$ (b) $l = 4$

FIGURE 13. $\tan\psi(m) = \frac{1-y(m)}{m}$ versus m

2.5. **A methodological remark.** When l is an integer, the fixed point of (1.1) $|y|^l + \frac{y}{m} - \frac{1}{m} = 0$, $m \neq 0$ are the roots of 1 (resp. 2) polynomials of degree l when l is even (resp. odd). From a computational point of view there is no need to restrict l to be an integer.

For $l > 0$, the solutions of (1.1) can be computed as the inverse map of $y \mapsto m = \frac{1-y}{|y|^l}$. This computing procedure will be used for $0 < l < 1$ or $l \geq 5$. The real solution $y(m)$ satisfies

$y(0) = 1$ and $y(2) = -1$ for all $l > 0$. By means of the inverse map $m(y)$, it is easy to show that $m_0 = -\frac{(l-1)^{l-1}}{l^l} = -\frac{1}{l}(1-\frac{1}{l})^{l-1}$ and $y(m_0) = \frac{l}{l-1} = 1 + \frac{1}{l-1}$ for $l > 1$. Hence, as $l \to \infty$, $m_0 \to 0^-$ and $y(m_0) \to 1 = y(0)$. Actually $|y(0)| \geq 1$ is arbitrary in the limit. Moreover, for $0 < m < 2$ $|y(m)| \approx 1$. For l fixed but large, $\lim_{m\to\infty} |y(m)| = 0$ is achieved extremely slowly.

Figure 14 displays $m \mapsto y(m)$ with a logarithmic scale for m in $[10^{-10}, 10^{300}]$ and $y \in [-1.5, 1]$, $l = 2^k$, $k = 3, 5, 6, 9, 10, 11$.

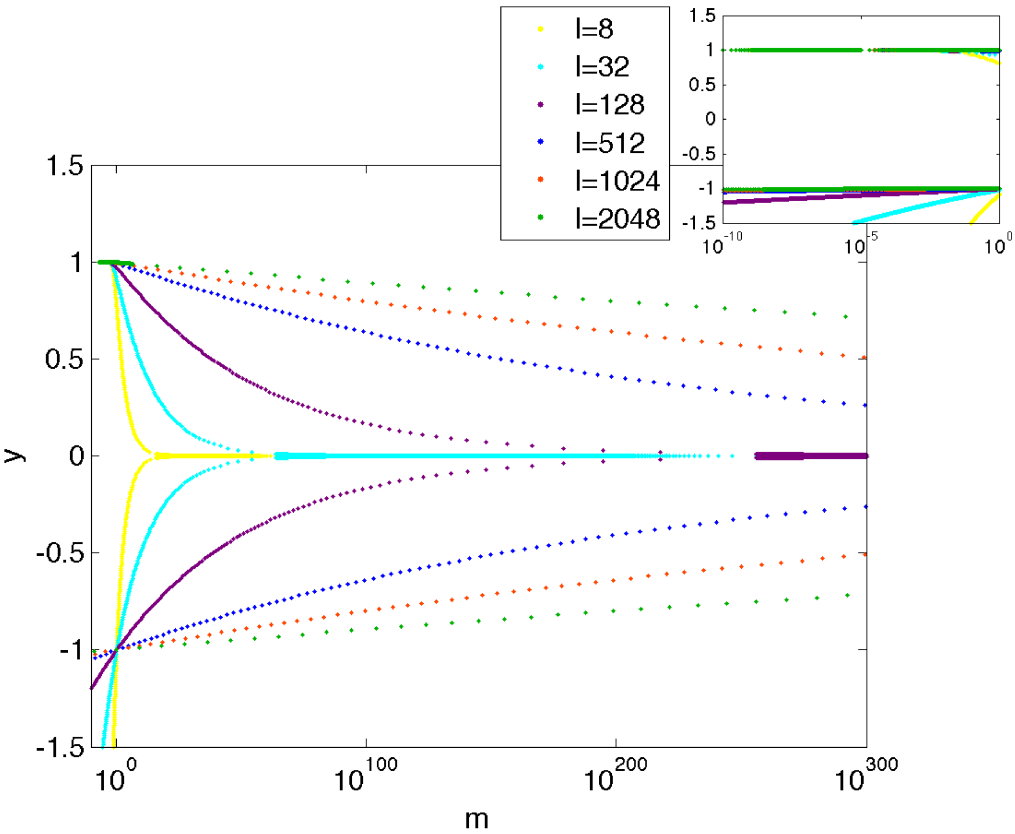

FIGURE 14. $m \in [10^{-10}, 10^{300}] \mapsto y(m)$

3. Numerical illustration of Picard iteration for $l = 1$ to 4

In Figure 15, the exact solutions $y(m)$ found in Section 2 for $l \in \{1, 2, 3, 4\}$ are plotted in red. These curves are compared with the Picard iterations given in (1.6) which are displayed in black in Figure 15. For $l = 2, 3, 4$ the superstable 2-cycle $(0, 1)$ is obtained for $m = 1$.

The quotient $\frac{y(m)-1}{m}$ is computed with the explicit values of $y(m)$ for $l = 1, 2, 3, 4$ and it is displayed in red in Figure 16. The quotient obtained for y given by the Picard iterations is plotted in black.

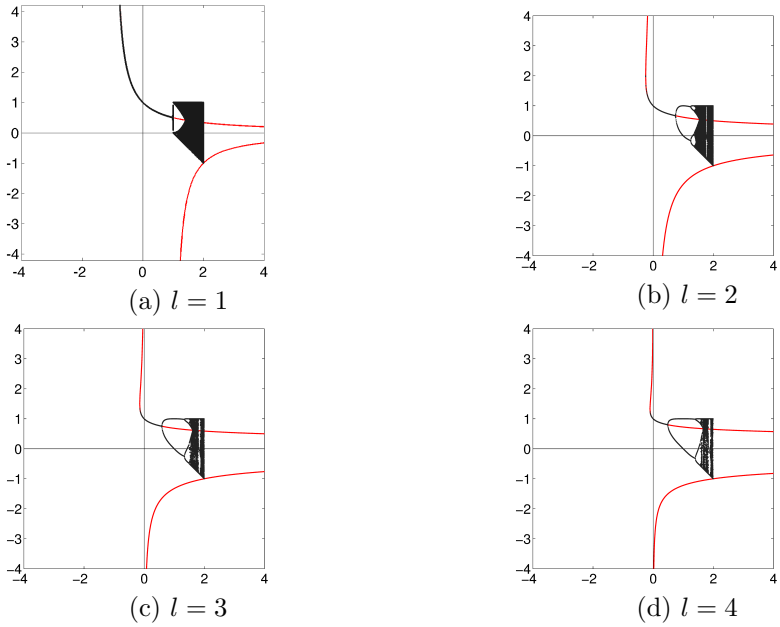

(a) $l = 1$ (b) $l = 2$

(c) $l = 3$ (d) $l = 4$

FIGURE 15. Orbit diagrams for fixed point iterations (black) and exact $y(m)$ (red)

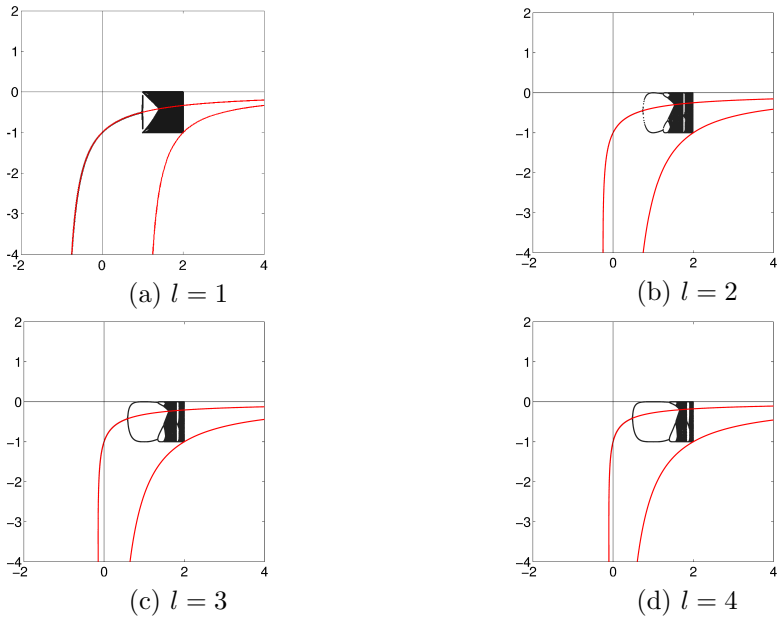

(a) $l = 1$ (b) $l = 2$

(c) $l = 3$ (d) $l = 4$

FIGURE 16. $\tan\psi(m) = \frac{y(m)-1}{m}$ versus m with explicit $y(m)$ (red) and Picard (black)

The relation $y(m) = \frac{x(m)}{m}$ which connects the solutions of (1.4) and (1.5) suggests to compare their orbit diagrams which display the *same* dynamics on $[-\frac{1}{4}, 2]$. On Figure 17 the vertical blue lines $m = \frac{3}{4}, \frac{5}{4}, \frac{7}{4}$ correspond to the bifurcations from period 1 and 2, 2 to 4 and 3.

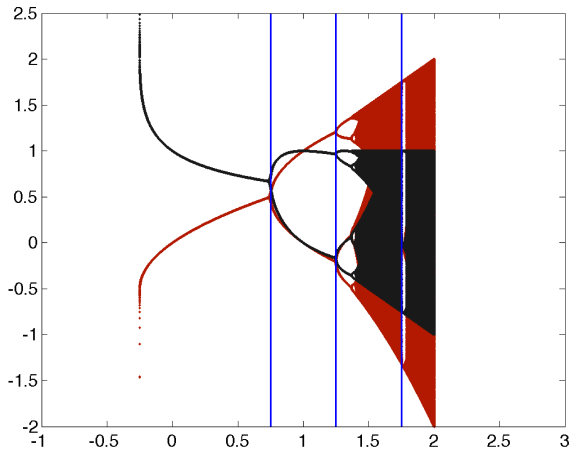

FIGURE 17. Orbit diagrams for (1.4) in black and (1.5) in red

Figure 18 offers a zoom for $m \in [1.75, 1.79]$ into the branch period 3 around the critical value $y = 0$.

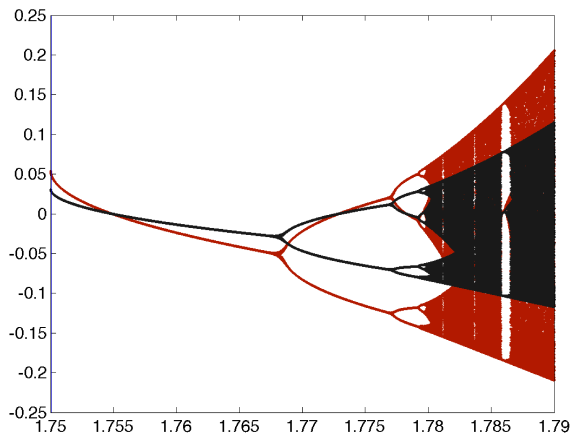

FIGURE 18. Zoom for period 3, $-0.25 < y_n < 0.25$

4. Numerical simulations on the Picard iteration for l positive

4.1. $0 < l < 1$. In the first row of Figure 19, the orbits diagrams are displayed for $l = \frac{1}{4}, \frac{1}{3}, \frac{1}{2}$ and $\frac{3}{4}$. We see that for $0 < l \leq l_1 < 1$, $l_1 \approx \frac{1}{2}$, the iterates do not escape to $-\infty$ at the right of the orbit maps. For $0 < l < 1$, one distinguishes the two isolated points $(1, 0)$ and $(1, 1)$ which define the 2-cycle for $G_l(1, \cdot)$: $\{0, 1\}$ are the fixed points of the composed function $G_l(1, G_l(1, \cdot))$.

The exact solutions y of (1.1) satisfy the inverse map $y \mapsto m = \frac{1-y}{|y|^l}$. Such curves are plotted in the second row of Figure 19 together with the orbit diagrams.

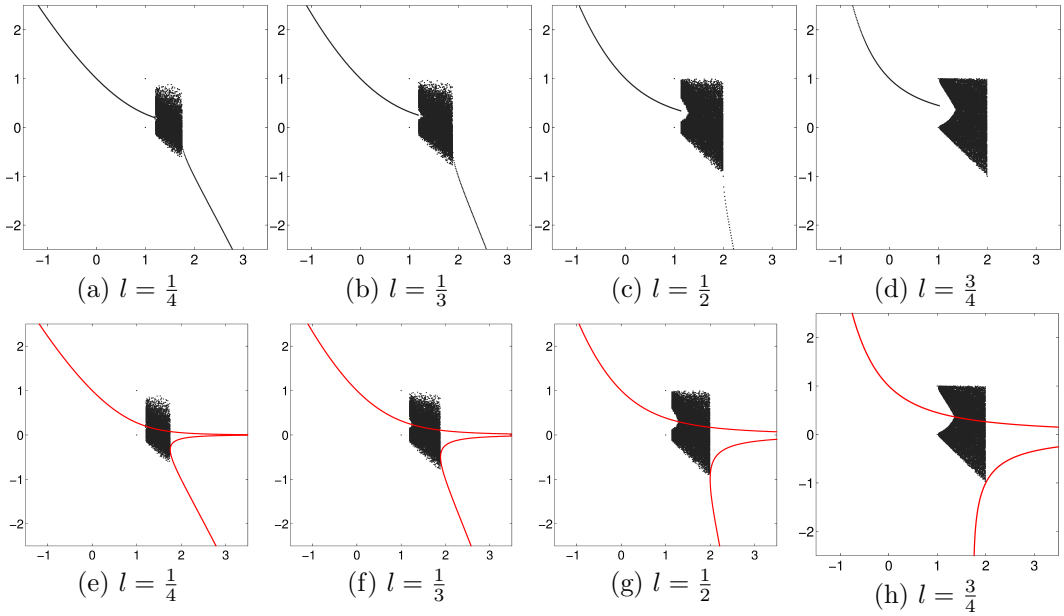

(a) $l = \frac{1}{4}$ (b) $l = \frac{1}{3}$ (c) $l = \frac{1}{2}$ (d) $l = \frac{3}{4}$

(e) $l = \frac{1}{4}$ (f) $l = \frac{1}{3}$ (g) $l = \frac{1}{2}$ (h) $l = \frac{3}{4}$

FIGURE 19. Orbit diagrams for the Picard iteration (black) and inverse map (red)

In Figure 20, the value of $\tan\psi$ is displayed in red when y is given by the inverse map and in black when y comes from the Picard iteration.

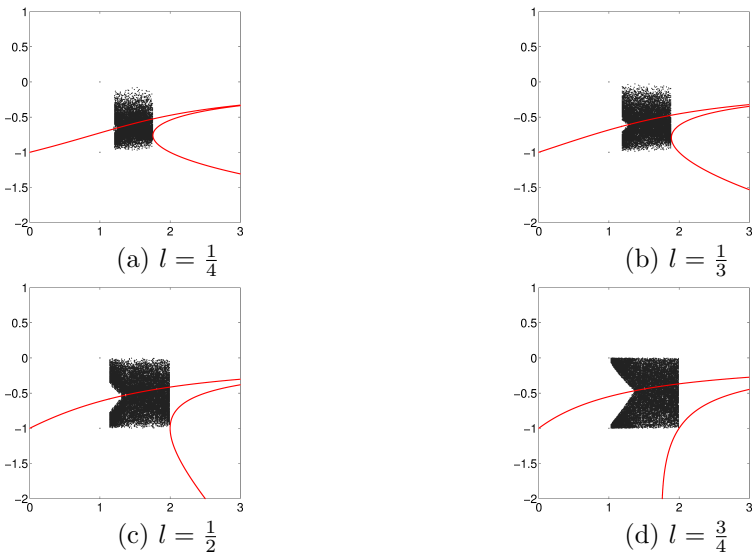

(a) $l = \frac{1}{4}$ (b) $l = \frac{1}{3}$

(c) $l = \frac{1}{2}$ (d) $l = \frac{3}{4}$

FIGURE 20. $\tan\psi(m) = \frac{y(m)-1}{m}$ versus m

4.2. l **large, display window** $[-0.5, 2.5] \times [-1.5, 1.5]$**.** The behaviour of the limit $l \to \infty$ is exemplified in Figure 21. The iterates do not escape to $\pm\infty$ iff $m \in [0, 2]$. They vary in $[-1, 1]$ for $m = 2$. For $m \in]0, 2[$, the iterates are confined by the two lines $y = 1$ and $y = 1 - m$. The

window of stability $[m_1, m_2]$ for the 2-cycle ($m_1 > 0$ and $m_2 < 2$) increases with l according to the table

l	2	3	4	64	∞
m_1	$\frac{3}{4}$	≈ 0.562	≈ 0.47	≈ 0.04	0^+
m_2	$\frac{5}{4}$	≈ 1.33	≈ 1.395	≈ 1.872	2^-

We shall see later that $m_1 \to 0^+$ and $m_2 \to 2^-$ as $l \to \infty$. Hence either the iterates oscillate between 1 and $1 - m$ for $0 < m < 2$, or they vary in $[-1, 1]$ for $m = 2$.

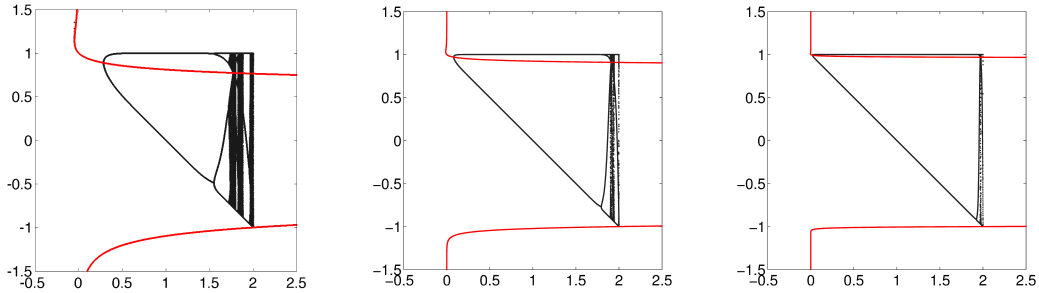

(a) $l = 8 = 2^3$ (b) $l = 32 = 2^5$ (c) $l = 128 = 2^7$

FIGURE 21. Orbit diagrams for fixed point iteration $l \geq 8$

The value of the quotient $\tan\psi(m) = \frac{y(m)-1}{m}$ based on the Picard iteration for the limit $l \to \infty$ is represented by $l = 512 = 2^9$ in Figure 22. For $m = 0$ and 2, ψ varies in $[-\frac{\pi}{4}, 0]$ and for $m \in]0, 2[$, $\psi \in \{-\frac{\pi}{4}, 0\}$.

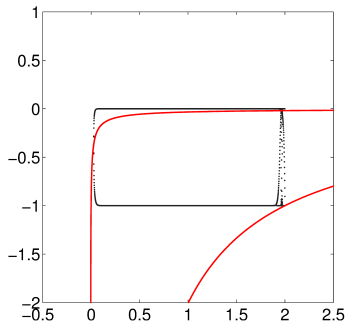

$l = 512$

FIGURE 22. $\tan\psi(m) = \frac{y(m)-1}{m}$ versus m, Picard iteration (black), exact (red)

4.3. **Numerical drift around m_0^-.** A detailed analysis of the behaviour of Picard iteration around the lower limit $m_0 < 0$ for the domain of the real solution $y(m)$ indicates that spurious values $y(m) > y(m_0)$ are computed for $m < m_0$, which differ significantly from the exact ones which are obtained for $m > m_0$. The computational artefact is illustrated on Figure 23 (a) (b) (c) (d) for $l = 2$, 3, 4, 8 respectively. Picard iterates appear in black, and the exact curve $m \geq m_0 \mapsto y(m)$ in red. This signals numerically that the upper branch $y > 1$, $m_0 < m < 0$ for the fixed point solution is theoretically unstable.

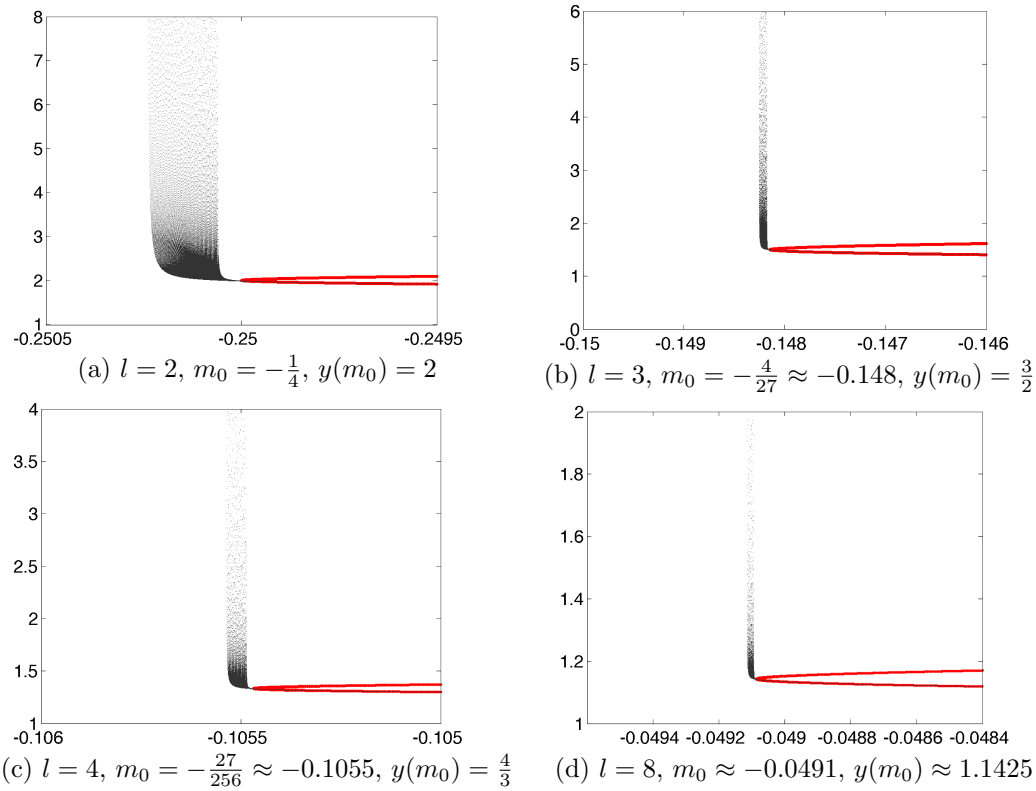

(a) $l = 2$, $m_0 = -\frac{1}{4}$, $y(m_0) = 2$ (b) $l = 3$, $m_0 = -\frac{4}{27} \approx -0.148$, $y(m_0) = \frac{3}{2}$

(c) $l = 4$, $m_0 = -\frac{27}{256} \approx -0.1055$, $y(m_0) = \frac{4}{3}$ (d) $l = 8$, $m_0 \approx -0.0491$, $y(m_0) \approx 1.1425$

FIGURE 23.

5. WAVETRACKS

In this work, the wavetracks (as they are called in [Chatelin, 2012, ch. 6]) are the curves $m \mapsto w_k(m)$, $k \geq 1$ with

$$\begin{cases} w_1(m) & = 1 - m|0|^l = 1, \quad w_2(m) = 1 - m, \\ w_{k+1}(m) & = 1 - m|w_k(m)|^l, \quad k \geq 2. \end{cases} \tag{5.1}$$

They are the successive iterates by $1 - m|y|^l$ of the critical point $y = 0$ where the first and second wavetracks do not depend on l: they differ for $m > 0$. For all n, $m \in [0, 2]$, $w_2(m) = 1 - m \leq y_n(m) \leq w_1(m) = 1$. The first four wavetracks are displayed on Figures 24, 26 and 27. One can check that for $m = 1$, $w_1 = w_3 = 1$, $w_2 = w_4 = 0$. The superstable 3-cycle $\{1 - \tilde{m}, 0, 1\}$ occurs for $\tilde{m}$, $1 < \tilde{m} < 2$ which solves $\tilde{m}(\tilde{m} - 1)^l = 1$, yielding $w_3(\tilde{m}) = 0$, $w_4(\tilde{m}) = 1$ and $w_5(\tilde{m}) = 1 - \tilde{m}$. For $l = 1$, $\tilde{m} = \frac{1+\sqrt{5}}{2}$ yields the 3-cycle $\{\frac{1-\sqrt{5}}{2}, 0, -1\}$. Interestingly, for $0 < m < 2 \Leftrightarrow |1 - m| < 1$, $w_3(m) = 1 - m|1 - m|^l$, converges to $w_1(m) = 1$ as $l \to \infty$. There are only *two distinct* wavetracks in the limit $l \to \infty$ on $]0, 2[$. This establishes that $m_1 \to 0^+$ and $m_2 \to 2^-$. As a corollary, the superstable 3−cycle tends to $\{-1, 0, 1\}$ at $m = 2$.

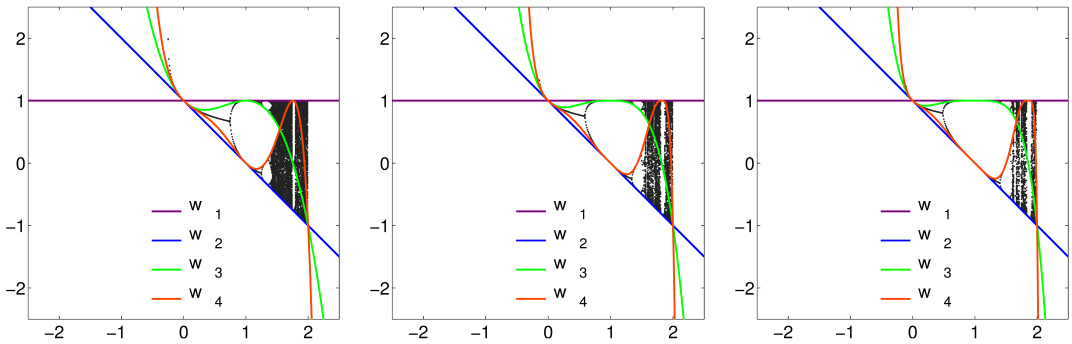

(a) $l = 2$ (b) $l = 3$ (c) $l = 4$

FIGURE 24. Smooth wavetracks $l = 2, 3, 4$

Figure 25 superimposes the 6 wavetracks w_{3i}, $i = 1$ to 6 inside the period-3 window for (1.4) and (1.5), see also Figure 18.

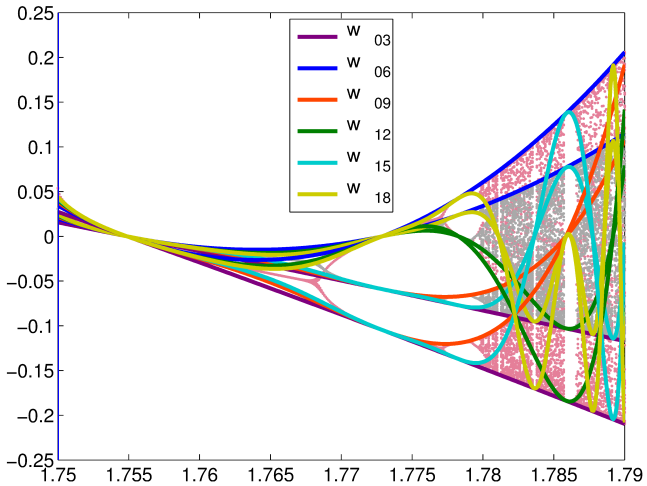

FIGURE 25. Wavetracks for (1.4) and (1.5), $l = 2$

For $0 < l \leq l_1$, $l_1 \approx \frac{1}{2}$, the lower bound $w_2 = 1 - m$ and the upper bound $w_1 = 1$ are not achieved by the iterates y_n; chaos occurs for $1 < m < 2$ only. The parameter l controls the smoothness of the wavetracks. For $l \leq 1$, the wavetracks present some cusps. By contrast they are everywhere smooth for $l > 1$.

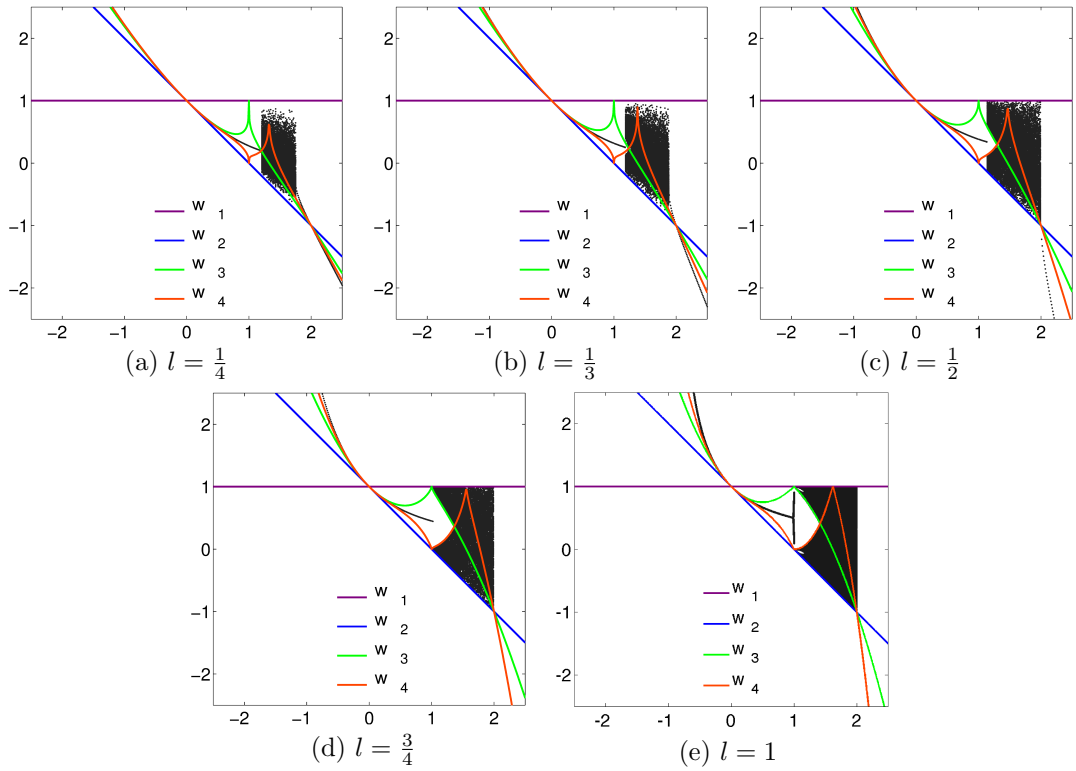

(a) $l = \frac{1}{4}$ (b) $l = \frac{1}{3}$ (c) $l = \frac{1}{2}$

(d) $l = \frac{3}{4}$ (e) $l = 1$

FIGURE 26. Continuous wavetracks for $0 < l \leq 1$

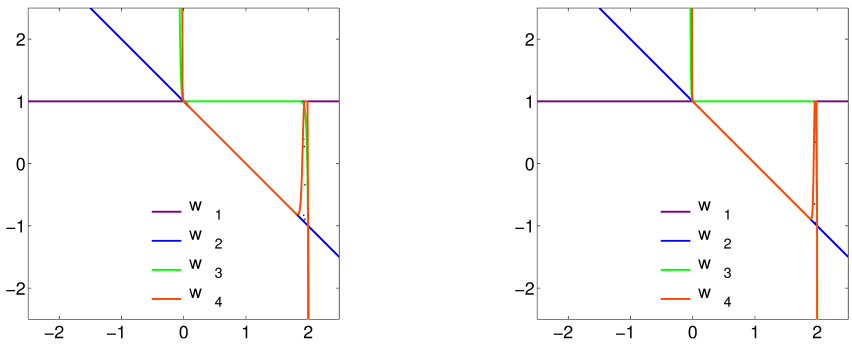

(a) $l = 50$ (b) $l = 100$

FIGURE 27. Wavetracks for l large

6. UNIVERSAL METRIC SCALINGS FOR $l \geq 2$, $l \in \mathbb{N}$

In [Feigenbaum, 1979], Feigenbaum observed that if for l integer, $l \geq 2$ and for a given value m, the sequence (1.6) is asymptotically periodic with period p, then if m is increased there is a bifurcation and a $2p$ period appears. Let m_j be the first value m where a 2^j-period appears on the Feigenbaum's route to chaos. The asymptotic scaling $\delta_l = \lim_{j\to\infty} \frac{m_j - m_{j-1}}{m_{j+1} - m_j}$, $\delta_2 \approx 4.669$

relating 2 consecutive bifurcation parameters m_j and m_{j+1} was conjectured by Feigenbaum to be a universal constant, depending only on l but *not* on the details of the function.

Another scaling constant is the limit ratio: $\alpha_l = \lim_{j\to\infty} \frac{d_j}{d_{j+1}}$, $\alpha_2 \approx -2.503$ where d_j is the value of the nearest cycle element to the critical value $y = 0$ in the 2^j superstable cycle [Feigenbaum, 1979].

The conjectures were proved for $l = 2$ in [Lanford III, 1982] and for $2 \le l \le 13$ in [Epstein, 1986]. Moreover, that $\alpha_1 = -\infty$ and $\alpha_\infty = -1$ (resp. $\delta_1 = 2$, $\lim_{l\to\infty} \delta_l$ exists at a value close to 30) is proved in [Delbourgo, 1992] (resp. [Collet et al., 1980, Van Der Weele et al., 1986]). Next [Eckmann and Epstein, 1990] showed that $29.5128 < \delta_l < 29.9571$ for l large enough. Even though δ_l and α_l assume the theoretical values 2 and $-\infty$ for $l = 1$. we recall that *no* period is observable (the Schwarz derivative is 0). Finally the estimate $\delta_\infty = 29.576303 \pm 10^{-6}$ is given in [Briggs, 1997, p.35].

The constants were calculated to high precision in [Briggs, 1991] and they are plotted in Figure 28 (a) and 29 (a) for α_l and δ_l respectively, $l \le 12$, to form piecewise linear curves.

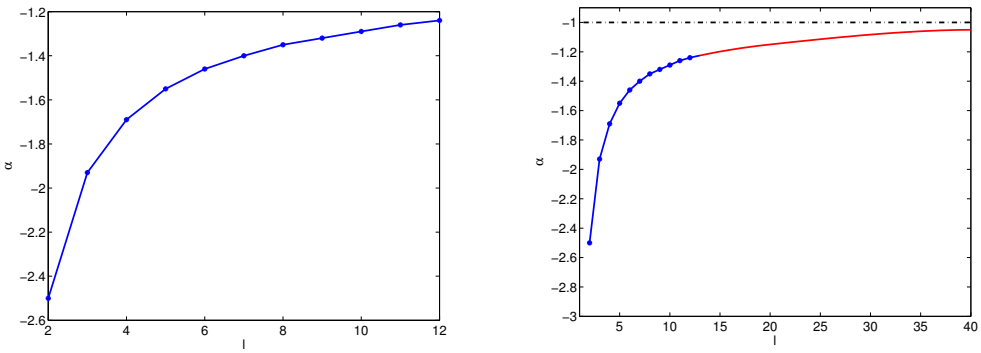

(a) $2 \le l \le 12$ (b) $2 \le l \le 40$

FIGURE 28. α_l versus $l \ge 2$

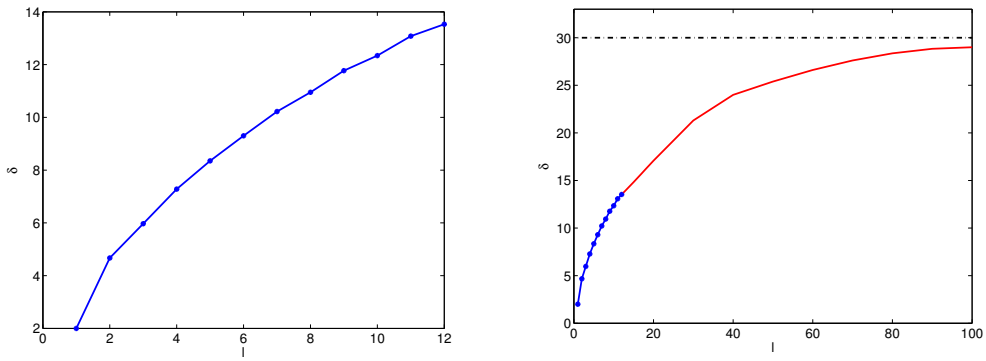

(a) $1 \le l \le 12$ (b) $1 \le l \le 100$

FIGURE 29. δ_l versus $l \ge 1$

On Figures 28 and 29 ((b) right) the computed curves on the left have been tentatively extrapolated for $l \geq 13$, using the theoretical predictions that $\alpha_\infty = -1$ and $\delta_\infty \approx 30$. The extrapolation appears in red.

7. Comparative analysis of the numerical simulations

The universal character of the dynamics of Picard iteration was established in the decades 1980s and 1990s. It is overall confirmed by the numerical simulations performed on (1.1) and (1.2) for $l \geq 2$. We observe that the dynamics differ for $0 < l < 1$. The isolated point $(\frac{1}{2}, \frac{1}{2})$ obtained for $l < 1$ in Figure 18 of [Rincon-Camacho et al., 2014a] is the superstable *fixed point* of (1.2). By contrast the two isolated points $(1, 0)$ and $(1, 1)$ which show on Figure 19 here form the superstable *2-cycle* for (1.1). Moreover there is no counterpart for (1.1) to the slow emergence of the forward chaos for (1.2) when $\frac{1}{2} \leq l < 1$ (Figure 20 in [Rincon-Camacho et al., 2014a]).

This significant difference persists for $l > 1$. For l very large: the Picard iteration on (1.1) converges almost everywhere for $m \in [m_0, 2[$ to the *2-cycle* $\{1 \text{ or } 1 - m\}$, whereas on (1.2) it converges almost everywhere for $h \in [h_0, 1[$ to the *fixed point* (or 1-cycle) $\{x = \mathbf{1}\}$. The exact solution $x = \mathbf{0}$ is not realised by successive iteration for l very large unless $|h|$ is very small. Moreover neither $\lim_{(l,|h|)\to\infty} x(h) = 1$ nor $x = 0$ presents any problem at $|h| = \infty$ whereas $\lim_{m\to\infty} y(m) = 0$, $l < \infty$ (Figure 14) and $\lim_{l\to\infty} |y(m)| = 1$, $m < \infty$ (Figure 21). There is a clash of limits when l and m become infinite.

Figures 30 and 31 display sketches for $\lim_{l\to\infty}$.

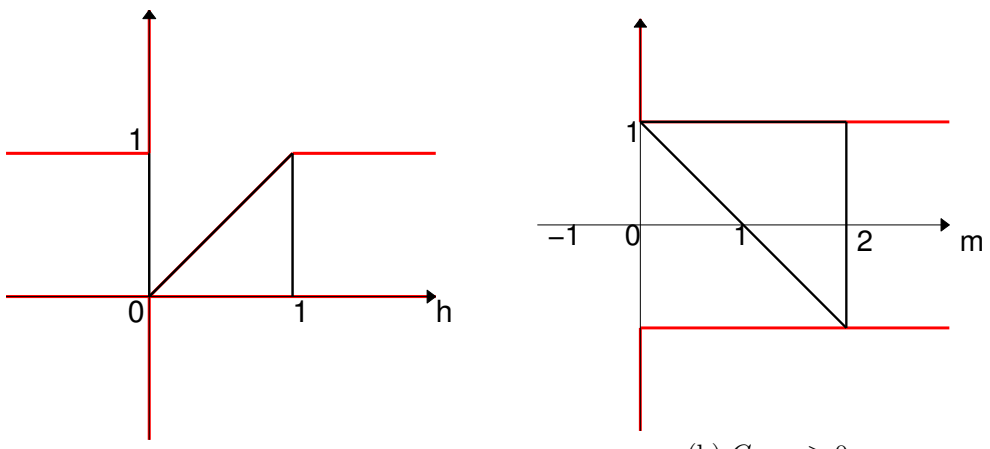

(a) Λ_h, $h \in \mathbb{R}$ (b) G_l, $m \geq 0$

Figure 30. At $l = \infty$: Picard (black), exact (red).

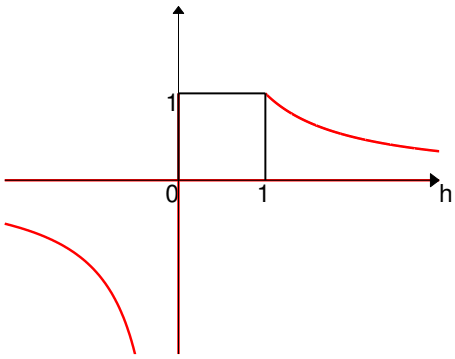

(a) $\tan\theta(h)$, $h \in \mathbb{R}$

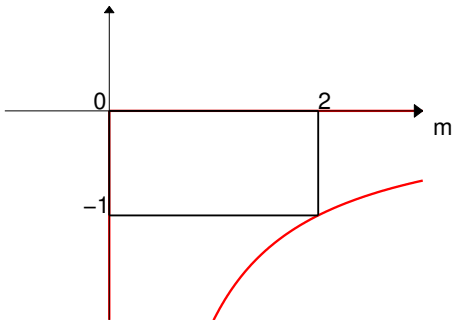

(b) $\tan\psi(m)$, $m \geq 0$

FIGURE 31. $l = \infty$, Picard (black), exact (red).

8. Conclusions

This work is the companion research report for [Rincon-Camacho et al., 2014a]. Taken together, they study an absolute and relative approach to the evolution of the numbers 0 and 1, the two fixed points of real multiplication. The evolution is based on the modification of $\times$, a linear map over certain real algebras of dimension 2^k, $k \geq 0$, to become the composition of continuous functions, a nonlinear map denoted $\circ$.

The evolution, whether it is absolute or relative, fulfills two different goals as $l \to \infty$. The *absolute* one aims at providing a *choice* between two answers on $[0, 2]$: either the constant function equals to the unit 1, or the map $m \mapsto 1 - m$ which represents the function $1 - \mathbf{1}$. The *relative* evolution, by contrast, tends to deliver the *unique* answer consisting of the identity function $\mathbf{1}$ on $]0, 1[$. It is significant that in the absolute (resp. relative) case, the derivative belongs to $\{0, -1\}$ (resp. is 1).

Acknowledgement M. M. Rincon-Camacho is grateful for the financial support from the Scientific Direction TOTAL through the contract DS-2755-B with Cerfacs (Qualitative Computing group).

References

[Boole, 1854] Boole, G. (1854). *An investigation into the laws of thought*. Walton and Maberly, London. [Reprinted (1951) Dover, New York.].

[Briggs, 1991] Briggs, K. (1991). A precise calculation of the Feigenbaum constants. *Mathematics of Computation*, 57(195):435–439.

[Briggs, 1997] Briggs, K. M. (1997). *Feigenbaum scaling in discrete dynamical systems*. PhD thesis, department of mathematics, University of Melbourne.

[Bronstein and Semendiaev, 1990] Bronstein, I. N. and Semendiaev, K. (1990). *Aide-mémoire de mathématiques*. Eyrolles, Paris.

[Chatelin, 2012] Chatelin, F. (2012). *Qualitative Computing: a computational journey into nonlinearity*. World Scientific, Singapore.

[Chatelin, 2014] Chatelin, F. (2014). An approach through Homotopic Deviation for the algebraic evolution of the numbers 0 and 1. Technical report, CERFACS (in preparation).

[Chatelin, 2015] Chatelin, F. (2015). Qualitative Computing, chapter 13 in *The human face of Computation. Conversations with famous scientists* (C. Calude ed.) . World Scientific and ICP, pages 163–179, also CERFACS TR/PA/14/56.

[Chatelin and Rincon-Camacho, 2014] Chatelin, F. and Rincon-Camacho, M. M. (2014). Organic Information Theory: living and feeling beyond the boolean world. Submitted to *Frontiers in Neuroscience*.

[Collet et al., 1980] Collet, P., Eckmann, J.-P., and Lanford III, O. (1980). Universal properties of maps on an interval. *Communications in Mathematical Physics*, 76(3):211–254.

[Delbourgo, 1992] Delbourgo, R. (1992). Relations between universal scaling constants in dissipative maps. *Nonlinear dynamics and chaos, Fourth Physics Summer School, Canberra 1991*, pages 231–256.

[Eckmann and Epstein, 1990] Eckmann, J.-P. and Epstein, H. (1990). Bounds on the unstable eigenvalue for period doubling. *Communications in Mathematical Physics*, 128(2):427–435.

[Epstein, 1986] Epstein, H. (1986). New proofs of the existence of the Feigenbaum functions. *Communications in Mathematical Physics*, 106(3):395–426.

[Feigenbaum, 1979] Feigenbaum, M. J. (1979). The universal metric properties of nonlinear transformations. *Journal of Statistical Physics*, 21(6):669–706.

[Gödel, 1931] Gödel, K. (1931). Über formal unentscheidbare Sätze der Principia Mathematica und verwandter Systeme I. *Monatshefte für Mathematik und Physik*, 38(1):173–198.

[Hirzel, 2000] Hirzel, M. (2000). On formally undecidable propositions of Principia Mathematica and related systems 1 . http://www.research.ibm.com/people/h/hirzel/papers/canon00-goedel.pdf.

[Lanford III, 1982] Lanford III, O. E. (1982). A computer-assisted proof of the Feigenbaum conjectures. *Bulletin of the American Mathematical Society*, 6(3):427–434.

[May et al., 1974] May, R. M. et al. (1974). Biological populations with nonoverlapping generations: stable points, stable cycles, and chaos. *Science*, 186(4164):645–647.

[Nagashima and Baba, 1999] Nagashima, H. and Baba, Y. (1999). *Introduction to Chaos: Physics and Mathematics of Chaotic Phenomena*. IOP Publ., Bristol, UK.

[Rincon-Camacho, 2014] Rincon-Camacho, M. M. (2014). A model for relative evolution of 0 and 1, the 2 fixed points of multiplication (submitted). In *Proceedings of 13th Conference Zaragoza-Pau on Mathematics and its Applications*. Jaca, Sept. 15-18, 2014.

[Rincon-Camacho et al., 2014a] Rincon-Camacho, M. M., Chatelin, F., and Ricoux, P. (2014a). About a family of logistic equation based on a relative distance to $\frac{1}{2}$ raised to a positive power. Technical report, CERFACS TR/PA/14/55.

[Rincon-Camacho et al., 2014b] Rincon-Camacho, M. M., Chatelin, F., and Ricoux, P. (2014b). About relative and absolute logic evolutions under laws of degree 2 and 4 and in 4 dimensions at most. Technical report, CERFACS TR/PA/14/75.

[Van Der Weele et al., 1986] Van Der Weele, J., Capel, H., and Kluiving, R. (1986). On the scaling factors $\alpha(z)$ and $\delta(z)$. *Physics Letters A*, 119(1):15–20.